JACS
JOURNAL OF THE AMERICAN CHEMICAL SOCIETY

Subscriber access provided by ISTANBUL TEKNIK UNIV

Article

Zeolite-Inspired Low-*k* Dielectrics Overcoming Limitations of Zeolite Films

Salvador Eslava, Jone Urrutia, Abheesh N. Busawon, Mikhail R. Baklanov, Francesca Iacopi, Steliana Aldea, Karen Maex, Johan A. Martens, and Christine E. A. Kirschhock

J. Am. Chem. Soc., **2008**, 130 (51), 17528-17536 • DOI: 10.1021/ja8066572 • Publication Date (Web): 20 November 2008

Downloaded from http://pubs.acs.org on February 8, 2009

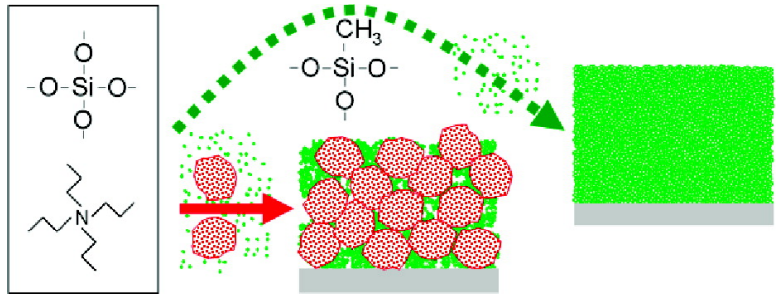

More About This Article

Additional resources and features associated with this article are available within the HTML version:

- Supporting Information
- Access to high resolution figures
- Links to articles and content related to this article
- Copyright permission to reproduce figures and/or text from this article

View the Full Text HTML

ACS Publications
High quality. High impact.

Journal of the American Chemical Society is published by the American Chemical Society. 1155 Sixteenth Street N.W., Washington, DC 20036

J|A|C|S
ARTICLES

Published on Web 11/20/2008

Zeolite-Inspired Low-*k* Dielectrics Overcoming Limitations of Zeolite Films

Salvador Eslava,[†,‡] Jone Urrutia,[‡] Abheesh N. Busawon,[§] Mikhail R. Baklanov,[‡] Francesca Iacopi,[‡] Steliana Aldea,[†] Karen Maex,[||] Johan A. Martens,[†] and Christine E. A. Kirschhock*[,†]

Centrum voor Oppervlaktechemie en Katalyse, Katholieke Universiteit Leuven, Kasteelpark Arenberg 23, 3001 Leuven, Belgium, IMEC, Kapeldreef 75, 3001 Leuven, Belgium, Department of Materials, Imperial College London, London SW7 2AZ, England, and ESAT-INSYS, Katholieke Universiteit Leuven, Kasteelpark Arenberg 10, 3001 Leuven, Belgium

Received August 22, 2008; E-mail: Christine.kirschhock@biw.kuleuven.be

Abstract: Spin-on zeolite films deposited from Silicalite-1 nanocrystal suspensions prepared by hydrothermal treatment of clear solutions have the required properties for insulating media in microelectronics. However, on the scale of the feature sizes in on-chip interconnects of a few tens of nanometers, their homogeneity is still insufficient. We discovered a way to overcome this problem by combining the advantages of the clear solution approach of Silicalite-1 synthesis with a sol−gel approach. A combination of tetraethyl orthosilicate and methyltrimethoxysilane silica sources was hydrolyzed and cocondensed in the presence of an aqueous tetraalkylammonium hydroxide template. The resulting suspension of nanoparticles of a few nanometers in size together with residual oligomeric silica species were spun onto support. The final zeolite-inspired low-*k* films (ZLK) with respect to pore size and homogeneity satisfied all requirements and presented excellent hydrophobicity, stiffness, and dielectric constant. The size and content of initially formed nanoparticles and the spatial hindrance promoted by occluded tetraalkylammonium molecules were found to be crucial elements in the definition of the final pore network.

Introduction

Films of MFI zeolite type known as Silicalite-1, deposited either by in situ crystallization[1] or by spin-on coating,[2−4] have interesting properties for insulating media in microelectronics. For future on-chip interconnects, spin-on Silicalite-1 zeolite films have dielectric constant (*k*) values below 3. Moreover, unlike most of other low-*k* materials, these films also show high elastic modulus and hardness.[5] Besides the potential of porous Silicalite-1 zeolite films for use in microelectronics, applications emerge in numerous fields of technology such as separation processes,[6,7] chemical syntheses,[8−11] and sensors.[12,13]

Spin-on Silicalite-1 zeolite films are typically deposited from Silicalite-1 suspensions prepared by hydrothermal treatment of clear solutions, which is extensively studied in the literature.[14−25]

[†] Centrum voor Oppervlaktechemie en Katalyse, Katholieke Universiteit Leuven.
[‡] IMEC.
[§] Imperial College London.
[||] ESAT-INSYS, Katholieke Universiteit Leuven.

(1) Wang, Z. B.; Wang, H. T.; Mitra, A. P.; Huang, L. M.; Yan, Y. S. *Adv. Mater.* **2001**, *13*, 746.
(2) Wang, Z. B.; Mitra, A. P.; Wang, H. T.; Huang, L. M.; Yan, Y. S. *Adv. Mater.* **2001**, *13*, 1463.
(3) Li, Z. J.; Li, S.; Luo, H. M.; Yan, Y. S. *Adv. Funct. Mater.* **2004**, *14*, 1019.
(4) Mintova, S.; Bein, T. *Adv. Mater.* **2001**, *13*, 1880.
(5) Dubois, G.; Miller, R. D.; Volksen, W. In *Dielectric Films for Advanced Microelectronics*; Baklanov, M. R., Green, M., Maex, K., Eds.; John Wiley & Sons Inc.: England, 2007; Chapter 2.
(6) Coronas, J.; Falconer, J. L.; Noble, R. D. *AIChE J.* **1997**, *43* (7), 1797.
(7) Yu, M.; Falconer, J. L.; Amundsen, T. J.; Hong, M.; Noble, R. D. *Adv. Mater.* **2007**, *19*, 3032.
(8) Saracco, G.; Specchia, V. *Catal. Rev.—Sci. Eng.* **1994**, *36* (2), 305.
(9) McLeary, E. E.; Jansen, J. C.; Kapteijn, F. *Microporous Mesoporous Mater.* **2006**, *90*, 198.
(10) Lacheen, H. S.; Cordeiro, P. J.; Iglesia, E. *J. Am. Chem. Soc.* **2006**, *128*, 15082.
(11) Zones, S. I.; Chen, C. Y.; Corma, A.; Cheng, M. T.; Kibby, C. L.; Chan, I. Y.; Burton, A. W. *J. Catal.* **2007**, *250*, 41.
(12) Yan, Y. A.; Bein, T. *J. Am. Chem. Soc.* **1995**, *117*, 9990.
(13) Grahn, M.; Wang, Z.; Lidstrom-Larsson, M.; Holmgren, A.; Hedlund, J.; Sterte, J. *Microporous Mesoporous Mater.* **2005**, *81*, 357.
(14) Ravishankar, R.; Kirschhock, C. E. A.; Knops-Gerrits, P. P.; Feijen, E. J. P.; Grobet, P. J.; Vanoppen, P.; De Schryver, F. C.; Miche, G.; Fuess, H.; Schoeman, B. J.; Jacobs, P. A.; Martens, J. A. *J. Phys. Chem. B* **1999**, *103*, 4960.
(15) Kirschhock, C. E. A.; Ravishankar, R.; Verspeurt, F.; Grobet, P. J.; Jacobs, P. A.; Martens, J. A. *J. Phys. Chem. B* **1999**, *103*, 4965.
(16) Kirschhock, C. E. A.; Ravishankar, R.; Van Looveren, L.; Jacobs, P. A.; Martens, J. A. *J. Phys. Chem. B* **1999**, *103*, 4972.
(17) Kirschhock, C. E. A.; Ravishankar, R.; Jacobs, P. A.; Martens, J. A. *J. Phys. Chem. B* **1999**, *103*, 11021.
(18) Kirschhock, C. E. A.; Buschmann, V.; Kremer, S.; Ravishankar, R.; Houssin, C. J. Y.; Mojet, B. L.; van Santen, R. A.; Grobet, P. J.; Jacobs, P. A.; Martens, J. A. *Angew. Chem., Int. Ed.* **2001**, *40*, 2637.
(19) Kirschhock, C. E. A.; Kremer, S. P. B.; Grobet, P. J.; Jacobs, P. A.; Martens, J. A. *J. Phys. Chem. B* **2002**, *106*, 4897.
(20) Kremer, S.; Theunissen, E.; Kirschhock, C. E. A.; Jacobs, P. A.; Martens, J. A.; Herfs, W. *Adv. Space Res.* **2003**, *32*, 259.
(21) Kirschhock, C. E. A.; Kremer, S. P. B.; Vermant, J.; Van Tendeloo, G.; Jacobs, P. A.; Martens, J. A. *Chem.—Eur. J.* **2005**, *11*, 4306.
(22) Davis, T. M.; Drews, T. O.; Ramanan, H.; He, C.; Dong, J. S.; Schnablegger, H.; Katsoulakis, M. A.; Kokkoli, E.; McCormick, A. V.; Penn, R. L.; Tsapatsis, M. *Nat. Mater.* **2006**, *5*, 400.
(23) Aerts, A.; Follens, L. R. A.; Haouas, M.; Caremans, T. P.; Delsuc, M. A.; Loppinet, B.; Vermant, J.; Goderis, B.; Taulelle, F.; Martens, J. A.; Kirschhock, C. E. A. *Chem. Mater.* **2007**, *19* (14), 3448.

 10.1021/ja8066572 CCC: $40.75 © **2008 American Chemical Society**

The clear solutions are formed by mixing tetraethyl orthosilicate (TEOS) with aqueous tetra-*n*-propylammonium hydroxide (TPAOH), which functions as a structure directing agent leading to zeolitization. The hydrolysis and condensation of TEOS in the presence of high concentrations of TPAOH result in the immediate formation of colloidal TPA−silica nanoparticles of ~3 nm next to small amounts of silica oligomers in solution. During the crystallization (e.g., at 80 °C), Silicalite-1 nanocrystals form through speciation and subsequent aggregation of those colloidal nanoparticles. Therefore, thermally treated clear solutions contain Silicalite-1 nanocrystals of 40−80 nm next to residual colloidal TPA−silica nanoparticles of ~3 nm. The spin-on deposition of this type of suspensions and posterior calcination give rise to porous films that are composed of amorphous silica matrix embedding Silicalite-1 nanocrystals. Amorphous silica acts as adhesive and filler between the nanocrystals, so their presence defines the textural and mechanical properties of the films.[26,27] The properties of spin-on Silicalite-1 zeolite films can be tuned by modifying the synthesis conditions and by post-treatments.[26,27] Nevertheless, some fundamental limitations hamper the development of films, satisfying the requirements for low-*k* dielectrics:[28,29] (1) Films meeting the requirement of low *k* values contain pores a few tens of nanometers wide whereas widths smaller than 5 nm are mandatory.[26,30] (2) These films therefore also lack homogeneity on the scale of the feature sizes in on-chip interconnects (a few tens of nanometers). The two phases (nanocrystals and amorphous silica) also contribute to the films' inhomogeneity.[27] (3) The films are hydrophilic so that the presence of water drastically increases the dielectric constant in a humid atmosphere.[31,32]

The presence of silanol moieties in the amorphous silica matrix and on the surface of the nanocrystals accounts for the hydrophilicity of spin-on Silicalite-1 zeolite films.[31,32] This limitation is known to be overcome by three methods: addition of methyltrimethoxysilane (MTMS) to the zeolite synthesis to incorporate hydrophobic methyl groups in the skeleton;[33] post-treatment by vapor phase reaction with trimethylchlorosilane to functionalize films with hydrophobic trimethylsilyl groups;[2,32] and ultraviolet-assisted curing (UV curing) to condensate silanol moieties and methylate the pore surface through fragmentation of the occluded TPA.[31,34] The two last methods are known to reduce porosity, but some of the remaining pores are still larger than 5 nm in diameter.

The large pores in spin-on Silicalite-1 zeolite films stem from embedding zeolite nanocrystals of 40−80 nm in an amorphous silica matrix originating from the residual nanoparticulate silica. If this filler is present in insufficient amounts, interstitial voids between nanocrystals of a few tens of nanometers remain. But even if nanocrystals are embedded in a more abundant filler, such as developed elsewhere,[35,36] a lack of homogeneity remains. It should be noted that the size of the nanocrystals used is comparable to future on-chip interconnect feature sizes.[28] Therefore, the presence of nanocrystals jeopardizes implementation of these films because their properties cannot be uniform at the required length scale.[27] A different approach is necessary to keep similar low *k* values and high elastic modulus attributed to spin-on Silicalite-1 zeolite films while avoiding the presence of nanocrystals of 40−80 nm.

An in-depth characterization of spin-on Silicalite-1 zeolite films prepared with different ratios of amorphous silica and nanocrystals revealed the best textural and structural properties are obtained with high ratios of amorphous silica (higher than 80 wt %).[27] The small dimensions and flexibility of the colloidal TPA−silica nanoparticles (~3 nm)[23] allow extensive cross-linking across the structure, minimizing interstitial pores and satisfying on-chip interconnect requirements on textural properties.[26,27] Accordingly, these films with high amounts of amorphous silica also have the best mechanical properties, which are defined by the cross-linking between nanocrystals rather than by the properties of the crystals themselves.[27] Unfortunately, increasing the amount of the amorphous matrix also increases the silanol content and leaves less porosity in the final films. The lower porosity, the polarity of the silanol moieties, and the adsorption of water increase the *k* value (~4).[27] Neither silylation nor ultraviolet-assisted curing can remedy this setback because both treatments would decrease the porosity of such amorphous films, thereby hampering the achievement of low dielectric constants.[31,32] However, the addition of MTMS to the synthesis of these amorphous films to reduce hydrophilicity needs to be explored.

In this paper, we propose a sol−gel synthesis of low-*k* materials with all the advantages of using colloidal TPA−silica nanoparticles but with minimized hydrophilicity. Since this approach was inspired by the clear solution Silicalite-1 synthesis, we refer to the final material as zeolite-inspired low-*k* material (ZLK). This approach involves the hydrolysis and cocondensation of TEOS and MTMS in the presence of aqueous TPAOH and ethanol, in which synthesis conditions were optimized to avoid gelation or formation of large nanocrystals. The use of MTMS ensured hydrophobicity while the required electrical, textural, mechanical, and structural properties were obtained. Comparison to spin-on Silicalite-1 zeolite films allowed assessment of this approach. TPA organics in spin-on Silicalite-1 films were evacuated by traditional thermal treatment and by UV-assisted curing. Films prepared by the latter method were included in the comparison because they obtained the smallest pores. Finally, we studied the effects of using different tetraalkylammonium hydroxide (TAAOH) types and concentrations in the synthesis.

Experimental Section

The ZLK procedure consisted of a sol−gel process based on a mixture of TEOS (98%, Acros), MTMS (98%, Acros), double deionized (DDI) water, ethanol, and TPAOH (40%, Alfa-Aesar). The reactant mixture prepared in an autoclavable bottle had an initial

(24) Fedeyko, J. M.; Rimer, J. D.; Lobo, R. F.; Vlachos, D. G. *J. Phys. Chem. B* **2004**, *108*, 12271.
(25) Fedeyko, J. M.; Vlachos, D. G.; Lobo, R. F. *Langmuir* **2005**, *21*, 5197.
(26) Eslava, S.; Baklanov, M. R.; Neimark, A. V.; Iacopi, F.; Kirschhock, C. E. A.; Maex, K.; Martens, J. A. *Adv. Mater.* **2008**, *20*, 3110.
(27) Eslava, S.; Kirschhock, C. E. A.; Aldea, S.; Baklanov, M. R.; Iacopi, F.; Maex, K.; Martens, J. A. Microporous Mesoporous Mater, doi: 10.1016/j.micromeso.2008.09.027.
(28) International technology roadmap for semiconductors (2007).
(29) Murarka, S. P. In *Interlayer Dielectrics for Semiconductor Technologies*; Murarka, S. P., Eizenberg, M., Sinha, A. K., Eds.; Elsevier Inc.: London, England, 2003; Chapter 2.
(30) Ree, M. H.; Yoon, J. W.; Heo, K. Y. *J. Mater. Chem.* **2006**, *16*, 685.
(31) Eslava, S.; Iacopi, F.; Baklanov, M. R.; Kirschhock, C. E. A.; Maex, K.; Martens, J. A. *J. Am. Chem. Soc.* **2007**, *129*, 9288.
(32) Eslava, S.; Delahaye, S.; Baklanov, M. R.; Iacopi, F.; Kirschhock, C. E. A.; Maex, K.; Martens, J. A. *Langmuir* **2008**, *24*, 4894.
(33) Li, S.; Li, Z.; Medina, D.; Lew, C.; Yan, Y. S. *Chem. Mater.* **2005**, *17*, 1851.
(34) Iacopi, F.; Eslava, S.; Kirschhock, C. E. A.; Martens, J. A. Patents US2007/0189961, EP1816104, and JP2007210884.
(35) Su, R. Q. Ph.D. Thesis, Technical University of Munich, 2004.
(36) Larlus, O.; Mintova, S.; Valtchev, V.; Jean, B.; Metzger, T. H.; Bein, T. *Appl. Surf. Sci.* **2004**, *226*, 155.

ratio of 0.5 MTMS/0.5 TEOS/5 water/8 ethanol/0.2 TPAOH. This basic catalyzed sol−gel process induces formation of clustered globular structures, i.e., colloidal nanoparticles, in suspension.[5,37] The clear suspension was heated to a temperature of 50 °C in an oil bath and stirred at 250 rpm while maintaining the same temperature for 22 h. Suspensions were stable and did not gel after several months. To avoid the formation of striations in spin-on films due to low boiling point solvents present in suspensions (i.e., water, ethanol, and methanol), the aged suspension was subjected to a solvent substitution process with propylene glycol monopropyl ether (PGP) in a rotary evaporator at 60 °C.[38] Those suspensions were also stable over months. The sols were filtered through 200 nm PTFE filters and used for spin coating (spin-on). The deposition was done on Si p-type wafers and highly doped Si n-type wafers. The wafers (about 2.5 × 2.5 cm^2) were cleaned with distilled water, dried, and then placed on the spinner. The spinning parameters were a rotation speed of 2000 rpm, with an acceleration of 1300 $rpms^{-1}$ for a duration period of 30 s. After the spin-on deposition, the films were heated (or baked) on a hot plate at a temperature of 150 °C in air for 1 min. The final step was to cure (or calcine) the film in N_2 atmosphere at a temperature of 400 °C for 30 min. We refer to this film as the ZLK film.

The same procedure was adopted for preparation of films with different TAA cations in different concentrations. The structure directing agents were tetramethylammonium (TMA), tetra-*n*-propylammonium (TPA), and tetra-*n*-pentylammonium (TPeA). Commercial TAAOH diluted in water was used: TMAOH (25 wt %, Alfa-Aesar), TPAOH (40 wt %, Alfa-Aesar), and TPeAOH (20 wt %, Alfa-Aesar). The initial molar ratios used were 0.5 MTMS/0.5 TEOS/*x* water/18 ethanol/*y* TAAOH, with *y* varying between 0, 0.1, and 0.2. The initial water/Si molar ratio (*x*) was kept at 5, but it varied for TPeAOH systems due to the low concentration of the aqueous TPeAOH used; *x* was 7 and 14 for TPeAOH systems with *y* equal to 0.1 and 0.2, respectively. Upon mixting reactants, no heating or solvent substitution was done. Suspensions remain in ethanol, methanol, and water. We refer to the resulting films or suspensions as TAAOHy, according to the TAA molecule and its used concentration.

For comparison to the ZLK film, spin-on Silicalite-1 zeolite films were prepared following the method in ref 2. A clear solution was prepared with TEOS (98%, Acros), TPAOH (40%, Alfa-Aesar), ethanol, and water in an autoclavable bottle. The final ratio was 2.8 SiO/40 water/22.4 ethanol/1 TPAOH. The clear solution was stirred for 3 days and then heated up to 80 °C in an oil bath under stirring for 5 days. The Silicalite-1 suspension was centrifuged at 5000 rpm for 30 min and filtered through 200 nm PTFE filters. The Silicalite-1 nanocrystal content was 63 wt % of the present silicon, and the average nanocrystal size was 66 nm. The filtered Silicalite-1 suspensions were used for spin coating with spinning parameters 3300 rpm, 30 s, and 1300 rpm s^{-1}. After the spin-on deposition, the films were dried at 80 °C overnight before either calcination or UV-assisted curing, as described elsewhere.[31] The UV-assisted curing was performed at 425 °C in nitrogen atmosphere while simultaneously irradiating for 5 min with a microwave driven electrodeless bulb which emitted high-intensity broadband UV radiation. The calcination was done at 425 °C for 2−3 h in air atmosphere. We refer to these spin-on Silicalite-1 films as Sil and UV-Sil (calcined and UV-cured, respectively.)

Particle-size analysis on prepared suspensions at 25 °C was carried out by dynamic light scattering (DLS) on an ALV-NIBS high performance particle sizer and was corrected for variation in viscosity measured with an AMVn Anton Paar viscometer. pH in suspensions was measured at ∼22 °C using a Mettler Toledo SevenMulti S40 pH meter equipped with an InLab420 glass electrode. Water and toluene adsorption isotherms on films were obtained by monitoring the ellipsometric angles Ψ and Δ at 633 nm wavelength during the adsorption and desorption cycle at 20 °C (ellipsometric porosimetry, EP). Two models were used for the pore radius distribution calculated from toluene adsorption isotherms. Below pore radii of 1.1 nm, the Dubinin Raduskevitch theory was applied; for larger pores, the model was based on the Kelvin equation. Further details of the calculation of the isotherms and the pore radius distribution can be found elsewhere.[39,40] The average contact angle of 1 μL drops of double deionized water on the film surface at 20 °C was determined from a picture recorded with a camera and fitting of the curvature with the Young−Laplace equation. The chemical structure and connectivity of the films was characterized by Fourier transform infrared spectroscopy (FT IR, Biorad FTS-40) in nitrogen atmosphere. Spectra averaged over 64 scans were recorded in the region 4000−400 cm^{-1} with 4 cm^{-1} resolution. The dielectric constant (*k*) of the films at 100 kHz was measured by impedance analysis (HP4284A-LCR meter) in a MIS type capacitor (metal−insulator−semiconductor). The thickness for dielectric constant calculation was measured by spectroscopic ellipsometry in the region 350−850 nm (Sentech SE801). The elastic modulus and hardness on films was measured by nanoindentation in continuous stiffness measurement with a Berkovich tip for films of 400−600 nm thickness. Elastic moduli and hardness were obtained at 10% indentation depth to avoid surface effects. The Poisson's ratio was approximated to that of fused silica (0.18). Views of cross-section of films were obtained by scanning electron microscopy (SEM, W-filament, Philips X-30, 5 kV).

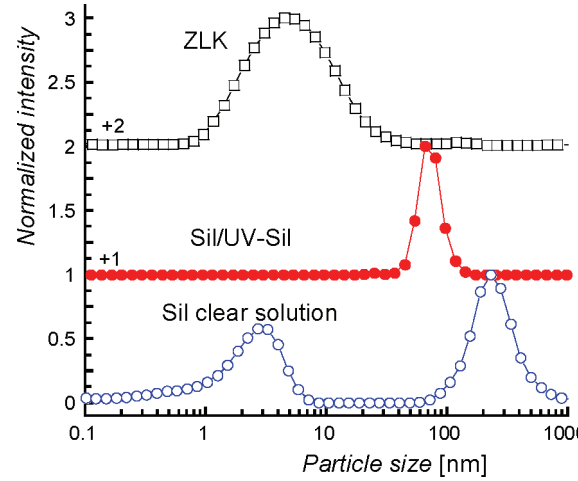

Figure 1. DLS particle size distribution of suspensions used for the deposition of Silicalite-1 zeolite films (UV-Sil and Sil) and ZLK film. The initial clear solution used for the preparation of Silicalite-1 zeolite suspension is also shown. For a clearer comparison, the origin of each distribution has been shifted by the indicated values.

Results and Discussion

Spin-Coating Precursors. The DLS particle size distributions (corrected for viscosity) at 25 °C on spin-coating precursors are shown in Figure 1. The initial clear solution used for the synthesis of Silicalite-1 nanocrystals had colloidal TPA−silica nanoparticles of ∼3 nm. Another signal corresponding to a particle size of ∼250 nm is attributed to aggregates of the nanoparticles. According to SEM, no rigid particles of ∼250

(37) Brinker, J.; Sherer, G. W. In *Sol-Gel Science—The Physics and Chemistry of Sol-Gel Processing*; Academic Press: San Diego, CA, 1990; Chapters 3 and 10.
(38) Kozuka, H. In *Handbook of Sol-Gel science and technology: Processing, characterization and application*; Sakka, S., Ed.; Kluwer Academic Publishers: Dordrecht, The Netherlands, 2005; Chapter 12.
(39) Baklanov, M. R.; Mogilnikov, K. P.; Polovinkin, V. G.; Dultsev, F. N. *J. Vac. Sci. Technol., B* **2000**, *18*, 1385.
(40) Grill, A.; Patel, V.; Rodbell, K. P.; Huang, E.; Baklanov, M. R.; Mogilnikov, K. P.; Toney, M.; Kim, H. C. *J. Appl. Phys.* **2003**, *94* (5), 3427.

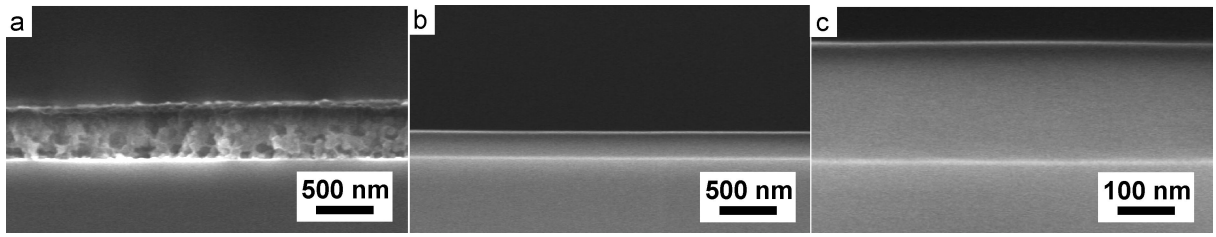

Figure 2. SEM images of (a) a spin-on Silicalite-1 film and (b and c) a ZLK film.

nm were present, indicating the aggregates to be of physical rather than of chemical nature (see next section). Although the DLS intensity of those ~250 nm aggregates was higher than that of ~3 nm nanoparticles, the concentration of the physical aggregates is minimal in a weight percentage due to the strong dependence of scattering power on particle size varying with particle radius to the sixth power.[41] After the heating period, the DLS analysis shows that ~3 nm nanoparticles were converted to a suspension of Silicalite-1 nanocrystals with 66 nm average size. Residual silica remained in the form of ~3 nm nanoparticles and oligomers but remained undetected by DLS analysis due to the very high signal intensity of the nanocrystal population. The ZLK approach containing MTMS next to TEOS gave rise to a population of colloidal nanoparticles with ~5 nm average size. These nanoparticles were TPA−organosilica composites, most probably resembling the nanoparticles found in clear solutions of Silicalite-1 synthesis. More detailed investigation of their structure and the influence of methyl groups is a subject of our future research.

Textural Properties of Films. A cross section of calcined films was inspected by SEM. Figure 2 shows images of a calcined spin-on Silicalite-1 film and a ZLK film. The spin-on Silicalite-1 film showed the presence of nanocrystals of 40−80 nm, in agreement with previous DLS analysis. It can be noted that these nanocrystals affected the homogeneity of the films on a scale of a few tens of nanometers (Figure 2a). On the other hand, the ZLK film showed no presence of nanocrystals or relatively large nanoparticles (Figure 2b and c). The films were very homogeneous at a scale of few tens of nanometers.

The crystallinity in films was studied by XRD in reflection mode. Figure 3 shows the patterns on spin-on Silicalite-1 films (UV-Sil and Sil) and on a ZLK film. The typical Bragg reflections of the MFI-type zeolite for the calcined and UV-cured Silicalite-1 films were observed.[42] On the other hand, the ZLK film showed no crystalline long-range order. This proved the Bragg-amorphous character of the film due to the absence of nanocrystals. However, FT IR spectroscopy showed that nanoparticles in ZLK synthesis also possess cyclic species with a similar vibration pattern to that of colloidal Silicalite-1 precursors. This is observed in Figure 4, showing FT IR spectra of a ZLK film at different steps of the preparation procedure: upon spin coating (20 °C), upon a 150 °C bake for 1 min, and after heating at 400 °C in nitrogen atmosphere for 30 min. Films that were not exposed to temperatures higher than 150 °C clearly showed a broad absorption band around 550 cm^{-1} that in Silicalite-1 precursors is attributed to pentasil structures that lack

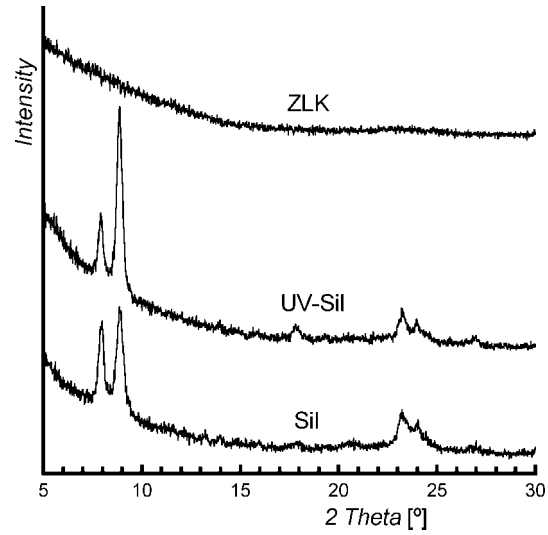

Figure 3. XRD patterns on spin-on Silicalite-1 films (calcined, Sil, and UV-cured, UV-Sil) and on a ZLK film.

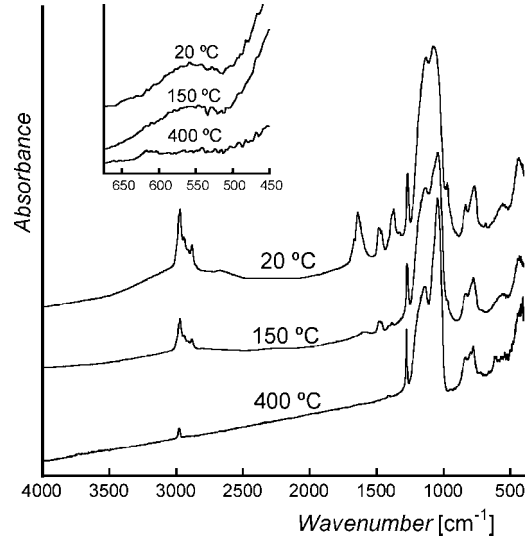

Figure 4. FT IR spectra in the region 4000−400 cm^{-1} of a ZLK film upon deposition (20 °C), upon a bake at 150 °C for 1 min, and after heating at 400 °C in nitrogen atmosphere for 30 min.

long reaching intercondensation (see inset in Figure 4).[43,44] Although this feature shows a likeness between nanoparticles in ZLK synthesis and Silicalite-1 precursors, further investiga-

(41) Feigin, L. A.; Svergun, D. I. In *Structure analysis by small-angle X-ray and neutron scattering*; Taylor, G. W., Ed.; Plenum Press: New York, 1987.
(42) Flanigen, E. M.; Bennett, J. M.; Grose, R. W.; Cohen, J. P.; Patton, R. L.; Kirchner, R. M. *Nature* **1978**, *271*, 512.
(43) Flanigen, E. M. In *Zeolite Chemistry and Catalysis*; Rabo, J. A., Ed.; American Chemical Society: Washington, DC, 1976; Vol. 171, pp 80−117.
(44) Lesthaeghe, D.; Vansteenkiste, P.; Verstraelen, T.; Ghysels, A.; Kirschhock, C. E. A.; Martens, J. A.; Van Speybroeck, V.; Waroquier, M. *J. Phys. Chem. C* **2008**, *112* (25), 9186.

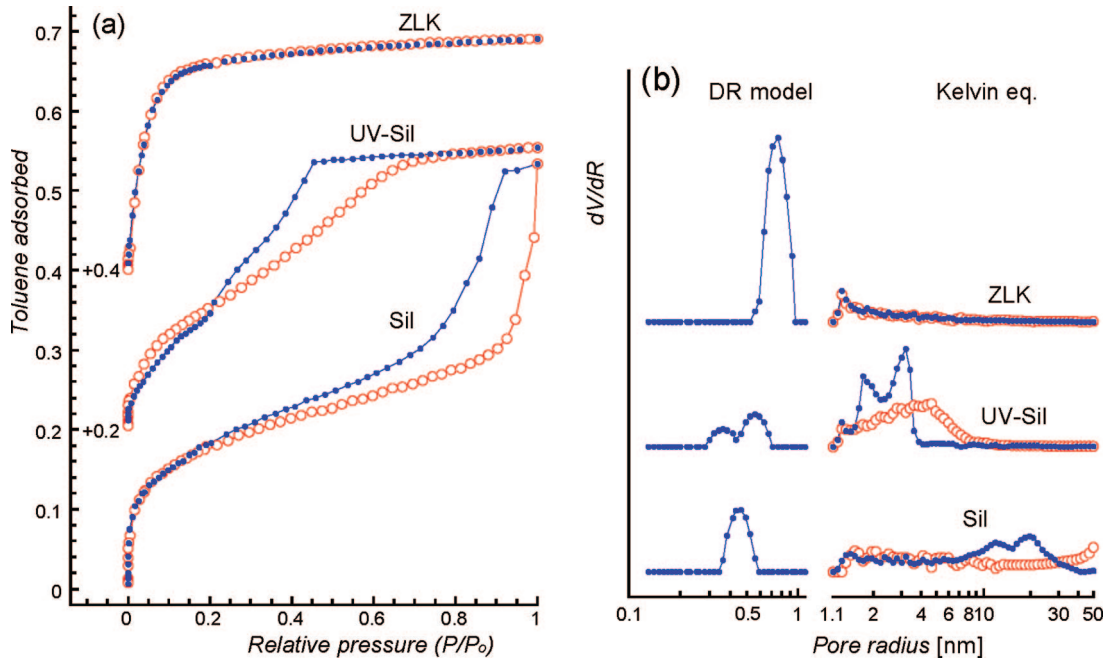

Figure 5. (a) EP toluene adsorption isotherms of spin-on Silicalite-1 films calcined (Sil) and UV-cured (UV-Sil) and on ZLK film. The *Y* axis shows the volume fraction of adsorbed toluene (vol_{tol}/vol_{film}). The isotherms were offset by the indicated values for a clearer comparison. (red circles) adsorption; (blue dots) desorption. (b) Pore radius distributions derived from the isotherms by applying models based on the Kelvin equation and Dubinin−Raduskevitch theory.

tion is needed to assess how methyl groups are distorting the structure of the nanoparticles. Upon heating at 400 °C, this IR absorption in ZLK films broadened substantially and covered the IR region 630−520 cm^{-1}. This indicates that in the calcined ZLK film a specific ring structure is not retained. Another feature observed upon heating at 400 °C is the disappearance of the broad C−H stretching vibration at approximately 3000 cm^{-1}. This confirms that the heating at 400 °C in nitrogen atmosphere for 30 min sufficed to evacuate the TPA cations.

The pore network of evacuated films was characterized using ellipsometric porosimetry (EP) and shown in Figure 5a. Toluene adsorption isotherms are compared for the following films: calcined spin-on Silicalite-1 film (Sil), UV-cured spin-on Silicalite-1 film (UV-Sil), and sol−gel film prepared with TPAOH (ZLK). Pore radius distributions (PRD) shown in Figure 5b were derived from the toluene adsorption isotherms using EP models based on Dubinin−Raduskevitch (DR) theory for pore radii smaller than ∼1.1 nm and the Kelvin equation for pore radii larger than ∼1.1 nm.[39,40] The reliability of these models has been assessed on porous films with monomodal PRD from ∼1 nm on.[40,45] Toluene adsorption isotherms on Silicalite-1 films (both Sil and UV-Sil) showed toluene uptake for a wide range of pressures, indicating a broad PRD from micro- to mesopores. Moreover, the hystereses between adsorption and desorption steps show that there were voids interconnected by narrower pore necks. In this situation, the Kelvin-based model used on the adsorption branch gives the PRD of the voids and, when used on the desorption branches, the PRD of the necks.[26] On the other hand, limitations appeared while analyzing such systems by the DR-based model in the radius range 0.1−1.1 nm. A Gaussian distribution is used to express the micropore PRD in DR theory,[46] so the broad PRD of micropores could not be described. Thus, the micropore radius in this PRD must be considered as a discrete average value of the micropore range (Figure 5b). These limitations probably account for the failure to observe the typical pores of Silicalite-1 (radius ∼ 0.3 nm), whose presence was confirmed by X-ray diffraction analysis (XRD, Figure 3). The largest void probed in spin-on Silicalite-1 was as high as ∼50 nm radius. The presence of interstitial voids between nanocrystals accounts for these large pores, as recently demonstrated elsewhere.[26] In the films prepared with a UV curing step, the packing of nanocrystals within the amorphous matrix was enhanced. This reduced interstitial cavities down to a maximum pore radius of ∼8 nm (Figure 5b). However, even the best results obtained by UV curing did not reduce maximum pore radii below the required upper pore radius of ca. ∼2.5 nm.[30] On the other hand, the ZLK approach resulted in a PRD with an average radius as small as 0.8 nm (Figure 5b). The I type isotherm and the single kink on the adsorption desorption branches confirmed the micropore size and the monomodal dispersion (Figure 5a). These pores were both interstitial nanoparticle voids and intraparticle pores, since TPA molecules were expected to be occluded in the organosilicate matrix. Although the total porosity in ZLK was inferior to that of Silicalite-1 films (∼30 vs >35 vol %), ZLK outperformed spin-on Silicalite-1 zeolite films with respect to porosity because of the superior pore radius distribution. Sketches in Figure 6 aim at representing the structure of the films.

Hydrophobicity. The hydrophobicity of the films was studied by contact angle measurements of water drops deposited on the top surface and by EP with water adsorbate. The average water contact angles on films surface are listed in Table 1 and corresponding water adsorption isotherms are shown in Figure 7. As studied elsewhere, the top film surface of Sil films was

(45) Kondoh, E.; Baklanov, M. R.; Lin, E.; Gidley, D.; Nakashima, A. *Jpn. J. Appl. Phys.* **2001**, *40*, L323.

(46) Gregg, S. J.; Sing, K. S. W. In *Adsorption, Surface Area and Porosity*, 2nd ed.; Academic Press: London, England, 1982.

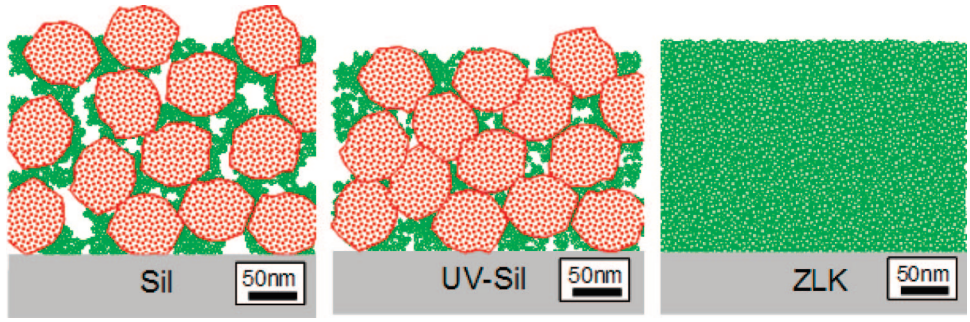

Figure 6. Sketch of spin-on Silicalite-1 films calcined (Sil) and UV-cured (UV-Sil) and a ZLK film, based on the results of DLS analysis and SEM images.

Table 1. Properties[a] of Spin-on Silicalite-1 Films Calcined (Sil) and UV-Cured (UV-Sil) and ZLK Film

	k (+ increase in air)	*E* (GPa)	*H* (GPa)	CA_{water} (deg)	*r* (nm)
calcined zeolite (Sil)	2.6 (+>300%)	6.2 (±1.5)	0.5 (±0.2)	10 (±5)	~0.3−50
UV-cured zeolite (UV-Sil)	2.2 (+5%)	10.7 (±3.2)	1.1 (±0.4)	137 (±11)	~0.3−8
zeolite-inspired low-*k* (ZLK)	2.2 (+0.5%)	6.8 (±0.3)	0.70 (±0.05)	92 (±1)	0.8

[a] *k* is the minimum dielectric constant measured upon degassing at 100 kHz; the increase in *k* upon exposure of the films to humid ambient is specified; *E* and *H* are the elastic modulus and hardness at 10% penetration depth in 400−600 nm films; CA_{water} is the average contact angle of water on the top surface of the films; and *r* is the pore radius measured on films.

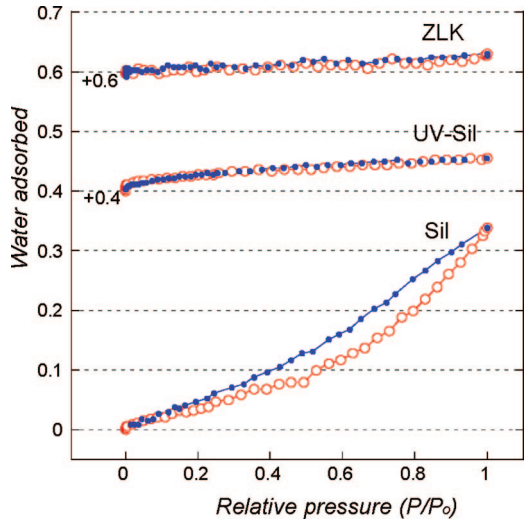

Figure 7. EP water adsorption isotherms on spin-on Silicalite-1 films calcined (Sil) and UV-cured (UV-Sil) and on ZLK film. The *Y* axis shows the volume fraction of water adsorbed (vol_{water}/vol_{film}). The origin of each isotherm has been shifted by the indicated values for a clearer comparison. (red circles) adsorption; (blue dots) desorption.

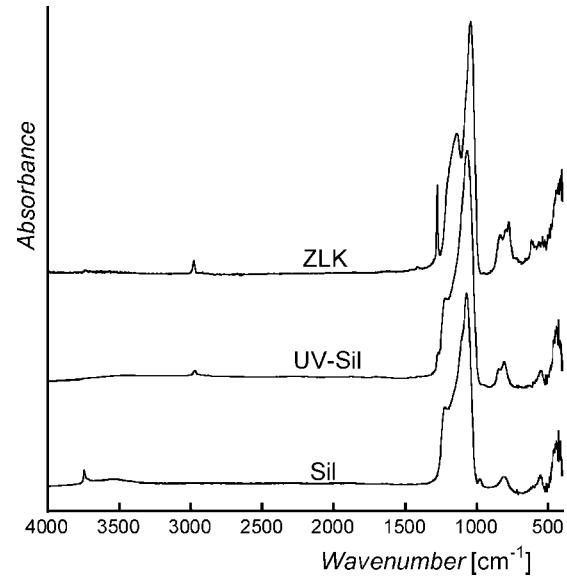

Figure 8. FT IR spectra in the region 4000−400 cm^{-1} of spin-on Silicalite-1 films calcined (Sil) and UV-cured (UV-Sil) and of calcined ZLK film.

very hydrophilic with a contact angle of ca. 10°.[31,32] The internal pore surface was less hydrophilic than the surface but still adsorbed water up to ca. 30 vol % at saturation pressure (Figure 7). When UV cured, both the top film surface and the internal pore surface were hydrophobic, as demonstrated elsewhere.[31] The hydrophobicity in UV-Sil is expressed in an average contact angle of ~140° and in the fact that water occupied only 5 vol % at saturation pressure (Figure 7). These values indicated that the top film surface was more hydrophobic than the internal pore surface. The higher UV field intensity on the film surface, revealed by a simulated standing wave pattern of light in a low-*k*, may account for these differences.[47] The ZLK film surface had a smaller water contact angle than UV-Sil, showing a lower surface hydrophobicity. However, the water adsorption isotherms characterizing the internal pore surface, which is more relevant for the electrical properties of the films, showed smaller water uptake (3 vol %) at saturation pressure (Figure 7). ZLK films can therefore achieve lower current leakage and lower deterioration of the electrical properties in a humid atmosphere.

The hydrophilic or hydrophobic character depends on the chemical structure and silicate connectivity, which was studied by FT IR analysis. The FT IR spectra of the films are shown in Figure 8. Common IR absorptions were assigned to different vibrations of Si−O bonds at 1020−1275 cm^{-1} (asymmetric stretching);[48] 800 cm^{-1} (symmetric stretching); and 450 cm^{-1} (bending). Differences between films were found in IR absorp-

(47) Eslava, S.; Eymery, G.; Marsik, P.; Iacopi, F.; Kirschhock, C. E. A.; Maex, K.; Martens, J. A.; Baklanov, M. R. *J. Electrochem. Soc.* **2008**, *155* (5), G115.

(48) Park, E. S.; Ro, H. W.; Nguyen, C. V.; Jaffe, R. L.; Yoon, D. Y. *Chem. Mater.* **2008**, *20*, 1548.

tion around 630−520 cm^{-1}. As shown above, the IR vibration of cyclic structures in nanoparticles of ZLK suspensions was affected during the 400 °C heating. However, in Silicalite-1 films (UV-Sil and Sil), the pentasil related vibration centered at 550 cm^{-1} remained upon curing because in the nanocrystals rings are preserved during the condensation process of the nanocrystals' outer surface with the amorphous filler, as also had to be expected from the diffraction experiments proving the presence of crystalline Silicalite-1 (Figure 3). Other differences were found at frequencies characteristic of OH vibrations: 3740−3450 cm^{-1} (silanols and physisorbed water) and 970 cm^{-1} (Si−OH stretching). UV-Sil and ZLK films had minimal absorption at those frequencies. This absence of silanol groups was in accordance with the observed hydrophobic character. Further differences were found at frequencies for organic moieties vibration: $C-H_x$ stretching (3000−2850 cm^{-1}); $C-H_x$ bending (∼1485 cm^{-1}); CH_3 symmetric bending in $Si-CH_3$ (∼1270 cm^{-1}); and Si−C stretching in $Si-CH_3$ (870−750 cm^{-1}). Sil film did not show any of these absorptions, as it contained no organic species after calcination. UV curing induced methylation of the pore surfaces, so UV-Sil showed organic-related vibrations.[31] As was expected, the ZLK film formed by the cocondensation of TEOS with MTMS showed these organic fingerprint vibrations very clearly, indicating a substantial content of organic groups. This explains the superior hydrophobicity of the ZLK film compared to UV-Sil, since a high concentration of nonpolar organic groups protect the pore surfaces against water activation, i.e., against hydrolysis of siloxane bridges.[49,50] For the same reasons, longer stability of the hydrophobicity in humid environments can be expected for ZLK films.

Dielectric Constant and Mechanical Properties. The dielectric constant of the films was investigated by impedance analysis on MIS structures. The lowest dielectric constants measured in a dry atmosphere are listed in Table 1. The minimum dielectric constant was lowest in UV-Sil and ZLK films (both with $k = 2.2$), because of the minimal amount of polar OH groups. Note that although the ZLK film had a lower porosity (Figure 5a), the increased number of $Si-CH_3$ groups with lower polarizability than Si−O groups contributed to a low dielectric constant.[51] The increase in dielectric constants in a humid atmosphere is also listed in Table 1. The hydrophilic Sil film had a significantly higher dielectric constant in a humid atmosphere (increase > 300%). UV-Sil showed only 5% increase. Finally, ZLK film had a marginal increase of 0.5%. As expected, the higher content of organic moieties ($Si-CH_3$) enhancing the hydrophobicity had beneficial effects on the electrical properties of ZLK film.

In addition to pore size, hydrophobicity, and chemical composition, which define the dielectric constant, the mechanical properties of materials are key issues for their implementation as low-*k* films. The elastic modulus (*E*) and hardness (*H*) are the typically studied mechanical properties. With respect to these properties, Silicalite-1 crystals are known to offer advantages due to their crystalline nature compared to amorphous porous materials.[52] However, the final mechanical properties in polycrystalline Silicalite-1 embedded in a matrix are defined by grain boundaries, interstitial volumes, and the amorphous matrix.[27,52] We measured the elastic modulus and hardness at 10% penetration depth in films with thickness 400−600 nm by nanoindentation. The values are shown in Table 1. The similar thicknesses of the studied films permitted the comparison. The nanoindentation analysis showed that the UV-Sil film showed the highest values of *E* and *H* because, in addition to a crystalline nature, the UV curing step optimized the packing of nanocrystals and amorphous silica, thus minimizing the effects of the composite nature of the film. ZLK films obtained lower *E* and *H*. However, in comparison to commercial low-*k*'s with similar dielectric constants, still superior values were achieved (6.8 vs < 4 GPa). Moreover, higher *E* and *H* are expected for UV-cured ZLK films. The high degree of internal cross-condensation in clustered nanoparticles during a base catalyzed sol−gel process ensured the good cross-linking of the final film matrix in ZLK, resulting in excellent mechanical properties.[53]

Porosity Dependence on TAA Size and TAAOH Concentration. Recently, we have shown the advantages of using tetraalkylammonium bromides (TAABr) as porogens in organosilicate systems prepared by an acid catalyzed sol−gel process.[54] In acid sol−gel synthesis of an organosilicate, a sol is formed containing a volume spanning a branched network of organosilicate chains. No nanoparticulate structures are formed. The good miscibility of TAABr in both the organosilicate sol and the final solid permitted nanocasting of monodispersed pores in the films. Moreover, the use of different alkyl chains in the TAA molecule and different TAABr concentrations tuned the final pore size and porosity. The molecules used were tetramethylammonium (TMA), tetra-*n*-propylammonium (TPA), and tetra-*n*-pentylammonium (TPeA), which yielded films with pore volumes between 18 and 54 vol % and pore radii between 0.6 and 1.8 nm. These TAABr molecules used as porogens outperformed other porogens that yielded larger pore radii. Based on these results, we evaluated the effects of differently sized structure directing agents in ZLK synthesis. The original ZLK synthesis contained TPAOH in a TPAOH/Si ratio of 0.2:1. As a next step, we used TMAOH, TPAOH, and TPeAOH in ZLK syntheses with *y* TAAOH/1 Si ratios with *y* varying between 0, 0.1, and 0.2. We refer to these films as TAAOH*y*, according to the used TAA molecule and TAAOH concentration. To permit a direct comparison between samples, the films were deposited without the additional solvent exchange applied in the original recipe (*cf.* Experimental Section).

First, we examined the nanoparticle formation in the ZLK suspensions by DLS analysis. In the absence of TAA ions (TAAOH0) the DLS pattern was featureless, indicating the absence of nanoparticles. Upon addition of TAAOH to the synthesis, nanoparticles were formed. The particle size distributions of TAAOH*y* films are shown in Figure 9, and average values are listed in Table 2. TMA0.1 was not measured because the sol gelled during the first hours of synthesis. For the measured TAAOH*y* samples, the particle average size lies between 1.7 and 6 nm depending on the used TAA cation. Like

(49) Eslava, S.; Baklanov, M. R.; Kirschhock, C. E. A.; Iacopi, F.; Aldea, S.; Maex, K.; Martens, J. A. *Langmuir* **2007**, *23* (26), 12811.
(50) Baklanov, M. R.; Mogilnikov, K. P.; Le, Q. T. *Microelectron. Eng.* **2006**, *83* (11−12), 2287.
(51) Maex, K.; Baklanov, M. R.; Shamiryan, D.; Iacopi, F.; Brongersma, S. H.; Yanovitskaya, Z. S. *J. Appl. Phys.* **2003**, *93*, 8793.
(52) Li, Z. J.; Johnson, M. C.; Sun, M. W.; Ryan, E. T.; Earl, D. J.; Maichen, W.; Martin, J. I.; Li, S.; Lew, C. M.; Wang, J.; Deem, M. W.; Davis, M. E.; Yan, Y. S. *Angew. Chem., Int. Ed.* **2006**, *45*, 6329.
(53) Wright, J. D.; Sommerdijk, N. A. J. M. In *Sol-Gel Materials Chemistry and Applications*; Gordon & Breach Science Publishers: Amsterdam, The Netherlands, 2001; Chapter 2.
(54) Eslava, S.; Baklanov, M. R.; Urrutia, J.; Kirschhock, C. E. A.; Maex, K.; Martens, J. A. *Adv. Funct. Mater.* **2008**, *18*, 3332.

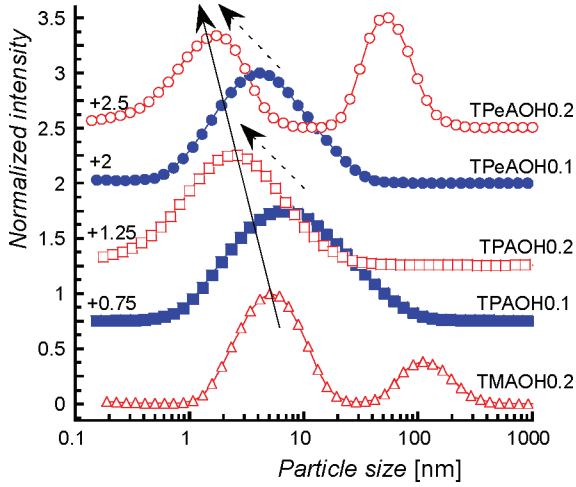

Figure 9. DLS particle size distribution on organosilicate suspensions prepared from different TAA types and TAAOH concentrations. For a clearer comparison, the origin of each distribution has been shifted by the indicated values.

Table 2. Characteristics of TAAOH*y* Suspensions

	Si/water ratio[b]	pH	DLS nanoparticle average size and fwhm[a] (nm)
TAAOH0	1:3.25	5.24	na
TMAOH0.1	1:3.25	gel	gel
TMAOH0.2	1:3.25	14.25	5.0, 8.6
TPAOH0.1	1:3.25	13.75	6.0, 26.3
TPAOH0.2	1:3.25	14.27	2.6, 6.9
TPeAOH0.1	1:5.25	13.45	4.1, 11.6
TPeAOH0.2	1:12.25	13.26	1.7, 2.8

[a] fwhm stands for full width at half-maximum. [b] Complete hydrolysis and cocondensation of Si sources is considered for the Si/water ratio.

in clear solutions used for Silicalite-1 nanocrystal formation (vide supra), some aggregates with relatively large size were observed. Those aggregates were not rigid, so of physical nature, and correspondingly, no evidence of them was observed in the final films. Nanoparticle size decreased with the increasing size of the TAA cations and also with increasing TAAOH concentration (see solid and dashed arrows in Figure 9, respectively, or Table 2).

Fedeyko et al. studied the formation of nanoparticles in similar systems consisting of 0−1.7 SiO_2/0.2−1.7 TAAOH/400 water/0−6.8 ethanol, after hydrolysis, by scattering techniques.[24,25] The best fit in the scattering analysis was obtained for core−shell oblate ellipsoidal particles with a silica-rich core surrounded by a TAA-rich layer. They demonstrate that after a critical aggregation concentration (cac), dependent on pH, the silica is present as nanoparticles in addition to a fraction of monomers and oligomers. The size and shape of nanoparticles is dependent on OH^- concentration and independent of the TAA cation type on those systems. Aerts et al. also studied those systems in a molar ratio of 28.6 SiO_2/5.7−21.7 TAAOH/400 water/114 ethanol, after hydrolysis, and found that with increasing OH^- concentration the nanoparticle content decreases in favor of the monomers and oligomers content.[23] That study considers the nanoparticles as a polydisperse population of charged colloidal silica−TAA species that are stabilized by a shell of the amphiphilic TAA cations. Increasing pH causes increasingly charged silica species that hinder the formation of these colloidal species, resulting in smaller nanoparticles in decreasing amounts compared to the oligomeric fraction.[23] The system studied here had substantially higher organic content in the solution due to

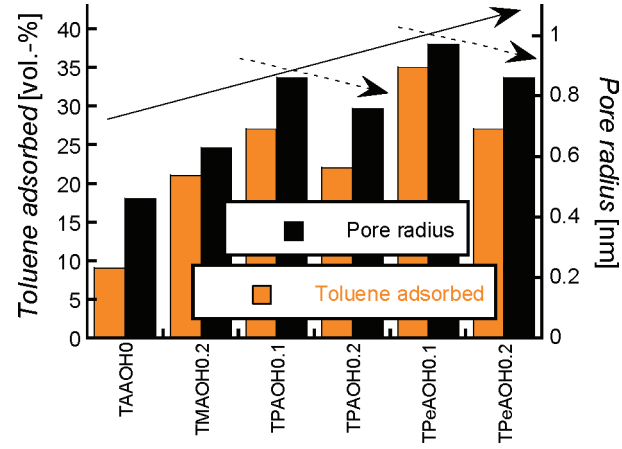

Figure 10. Results of EP measurements on organosilicate films prepared with different types of TAA cations and different TAAOH concentrations.

the use of ethanol as solvent and higher intrinsic hydrophobicity in the silicate fraction due to the MTMS content. Selecting as reference 400 mol of water, the studied molar ratios were 61.5 SiO_2/61.5 $SiO_{1.5}CH_3$/12−24 TAAOH/400 water/2460 ethanol/185 methanol, after hydrolysis. TPeAOH0.1 and TPeAOH0.2 had 646 and 1508 molecular amounts of water, respectively. In agreement with systems studied by Fedeyko and Aerts, the particle size shrank for higher pH in TPAOH*y* systems prepared with different TPAOH concentrations (Figure 9 and Table 2). The pH in the TPeAOH*y* systems only changed slightly upon changing the TAA amount. Still, significant changes in the particle distribution were observed. This could be due to the dilution effect, as water content also increased significantly,[55] or due to a true effect of changed Si/TPeA ratio. Unlike the systems studied by Fedeyko et al., the ZLK systems showed a dependence on the TAA organic cation type (see the solid line in Figure 9). The observed trends cannot be attributed to pH effects only (Table 2). Possibly, the higher organic content in the ZLK systems emphasized the role of the TAA organic cations, which is defined by their hydrophobic/hydrophilic interaction with silica species in solution.

Porosity in TAAOH*y* films was investigated by EP with toluene as adsorbate. In all films, the isotherm was a I type isotherm similar to that previously shown in Figure 5. The results of the EP toluene adsorption isotherms and calculated average pore radius are shown in Figure 10. Films prepared in the absence of TAAOH showed the inherent porosity of the organosilicate: a porosity of 9 vol % and an average pore radius of ∼0.5 nm. By using TAAOH, in the presence of nanoparticles, the film porosities and pore radii increased up to 35 vol % and 1 nm, respectively. The porosity increased with the TAA molecule size and decreased with the TAAOH concentration. The increase in porosity upon use of larger TAA cations was similar to that found in films nanocasted with TAABr molecules in acid conditions, where porosity increased from 9 to ∼50 vol %.[54] This leads to the conclusion that in basic conditions larger TAA cations also caused larger pores and increased porosity because of the higher volume they occupied during the film formation. But unlike the reported increase in porosity with increasing TAABr concentration in acid, these basic ZLK

(55) Follens, L. R. A.; Aerts, A.; Haouas, M.; Caremans, T. P.; Loppinet, B.; Goderis, B.; Vermant, J.; Taulelle, F.; Martens, J. A.; Kirschhock, C. E. A. *Phys. Chem. Chem. Phys.* **2008**, *36*, 5574.

systems decreased in porosity for higher TAAOH concentration, directly as a function of the decreasing size of nanoparticles (Figure 10) and decreasing amount of nanoparticles, as expected from Aerts' studies.[23] This was interpreted as a consequence of the presence of the globular structures, which can be packed more efficiently with decreasing particle size, and the varying amount of oligomeric species which serve as filler between the nanoparticles.

Conclusions

A new approach is proposed to prepare films that overcome the limitations found in spin-on Silicalite-1 zeolite films for on-chip applications. The approach is inspired by the first steps of the Silicalite-1 synthesis, where TEOS is hydrolyzed and condensed in the presence of a TPAOH structure directing agent forming a population of silica-template nanoparticles. To ensure hydrophobicity, MTMS is hydrolyzed and cocondensed with TEOS, which introduces $Si\text{-}CH_3$ groups already at the stage of the suspended nanoparticles. The resulting films are referred to as zeolite-inspired low-k (ZLK) films. Comparison of the final film properties of ZLK with those of spin-on Silicalite-1 zeolite films either calcined or UV-cured demonstrates the advantages of the ZLK approach for low-k dielectric applications. The pore radius of the ZLK films is about 0.8 nm. Homogeneity is achieved at the required length scale (~5 nm particle size). The internal hydrophobicity ensures excellent electrical properties ($k \sim 2.2$). The mechanical properties are not as outstanding as in UV-cured spin-on Silicalite-1 zeolite films but still are excellent for the implementation ($E = 6.8$ GPa and $H = 0.7$ GPa). The potential of the ZLK approach to tune porosity is evaluated on systems prepared with different TAAs in varying concentrations. Final porosity and pore size increase with the TAA size but decrease with the TAAOH concentration, as a result of the variation of nanoparticle structure and content in mixtures containing TAAOH. This study shows that insight into the colloidal properties of the starting solutions is an essential part of tuning the properties of the obtained films in a directed manner.

Acknowledgment. C.E.A.K. and J.A.M. acknowledge the Flemish government for a concerted research action (GOA).

JA8066572